






Multifrequency Phased-Arrays With Dynamic Range Ratio Control for Coastal Monitoring

Giulia Buttazzoni , Senior Member, IEEE, Fulvio Babich , Senior Member, IEEE, Alessandro Fanti , Senior Member, IEEE, Elena Marongiu, Student Member, IEEE, Francesca Vatta , Member, IEEE, and Massimiliano Comisso , Member, IEEE

Abstract—Coastal monitoring represents a key element for the support of many sea-related human activities, including ship navigation, national security prevention, and environmental protection. Within these fields, antenna arrays are recognized as viable candidates for the development of wide-area monitoring applications, thanks to the possibility of using multifrequency (MF) radiating systems as reflector feeds or as primary antennas. For this reason, this article proposes a deterministic synthesis method for MF antenna arrays allowing the independent pattern control at different frequencies. Precisely, the optimization of the array excitations is realized to provide a unique set of amplitudes, common to all frequencies, and S sets of phases, corresponding to the S considered frequencies, thus enabling phase-only pattern switching. The method, which is based on the alternating projection approach, allows also to impose an upper bound on the ratio between the maximum and the minimum amplitude, hence providing advantages in terms of feeding network simplification and energy efficiency, while maintaining satisfactory beam and null pointing capabilities. Numerical examples, including electromagnetic simulations, are presented to check the effectiveness of the conceived method for implementation in oceanographic acquisition systems.

Index Terms—Antenna arrays, dynamic range ratio (DRR) reduction, multifrequency (MF) antennas, phase-only control, power synthesis.

I. INTRODUCTION

COASTAL monitoring operations include a variety of critical tasks, ranging from homeland security to ocean protection, from ship detection to vessel tracking, from weather

Received 19 March 2024; revised 10 August 2024; accepted 13 August 2024. This work was supported in part by the European Union under the Italian National Recovery and Resilience Plan (NRRP) of NextGenerationEU, partnership on “Telecommunications of the Future” (PE00000001 - program “RESTART”). An earlier version of this paper was presented at the IEEE International Workshop on Metrology for the Sea (MetroSea2023), Oct. 2023. (Corresponding author: Giulia Buttazzoni.)

Guest Editor: M. Migliaccio.

Giulia Buttazzoni, Fulvio Babich, Francesca Vatta, and Massimiliano Comisso are with the Department of Engineering and Architecture, University of Trieste, 34127 Trieste, Italy, and also with the National Inter-University Consortium for Telecommunications, 50139 Florence, Italy (e-mail: gbuttazzoni@units.it; babich@units.it; vatta@units.it; mcomisso@units.it).

Alessandro Fanti is with the Department of Electrical and Electronic Engineering, University of Cagliari, 09123 Cagliari, Italy, and also with the National Inter-University Consortium for Telecommunications, 50139 Florence, Italy (e-mail: alessandro.fanti@unica.it).

Elena Marongiu is with the Department of Electrical and Electronic Engineering, University of Cagliari, 09123 Cagliari, Italy (e-mail: e.marongiu10@studenti.unica.it).

Digital Object Identifier 10.1109/JOE.2024.3450550

surveillance to geophysical parameters acquisition, such as surface temperature as well as wind, current, and wave velocities. Many of these activities can be performed by remote sensing systems, among which a great interest is devoted to the microwave (μ Wave) and millimeter wave (mmWave) ones relying on aerial platforms and satellites. In fact, at μ Wave and mmWave frequencies, the carrier wavelengths are, on the one hand, sufficiently long that signals propagate through atmospheric agents with negligible attenuation, and, on the other hand, sufficiently short that high-resolution imagery can be obtained [1].

For a long time, traditional acquisition systems have experienced limits in spatial resolution and geographical coverage due to the intrinsic limitations of the employed antenna technologies. So, in [2] the metrics for assessing the radars performance was investigated and the advantages provided by independent observations have been revealed. In particular, the adoption of different frequencies has been proposed as a valuable diversity technique for performance improvement. Similarly, it has been shown in [3] that an optimal multifrequency (MF) design of a phased array feed can lead to a major performance improvement over the traditional single-horn systems. Then, as phased-arrays have become more suitable for a broader variety of services, their possible use in the ocean engineering context has been considered increasingly attractive, thanks to their great versatility in satisfying complex beamforming specifications when applied to systems with a large number of radiating elements [3], [4]. Electronic beam steering, adaptive beam/null synthesis, and reconfiguration capabilities represent some of the features making them useful for oceanographic and radar applications. Accordingly, in [5], μ Wave X-band marine radars were used as wide coverage monitoring systems to acquire wave and current velocities with high resolution. A high-frequency (HF) surface wave radar was also proposed in [2], to enable maritime situational awareness in vessel monitoring networks covering wide coastal areas.

Beside phase-only control, MF operation has been identified as a further relevant feature to be supported in oceanographic equipment. In fact, still in HF surface wave radars, the frequency diversity reduces the probability of ship obscuration by wave echoes, simultaneously increasing the probability of hitting a high cross section [2]. Next generation radar systems are hence expected to implement reconfigurable MF arrays to exploit the same aperture over two or more frequency bands. By consequence, several multiband or ultra-wideband antenna designs

for MF operations have been recently developed. In particular, in [6], a planar dual-band wide-scan phased-array for X-band radar applications was presented. In [7], the authors proposed a μ Wave feed array covering three operational frequencies in the C, X, and Ku bands to accomplish multitask missions. The same work takes into account the beam efficiency through an iterative optimization procedure that enables the control of the dynamic range ratio (DRR), representing the ratio between the maximum and the minimum amplitude of the excitations [8]. Moreover, a synthetic aperture radiometer operating at 55 and 183 GHz for Earth observing applications was conceived in [9].

Within the antenna research field, many other synthesis methods for multiband, wideband, and ultrawideband frequency invariant arrays have been derived in the recent years [10], [11], [12]. Compressive sensing was specifically used in [13], to provide a design technique for MF sparse arrays. An innovative approach based on genetic algorithms was instead adopted in [14], to optimize the distribution of the antenna elements operating at different frequencies and sharing the same physical aperture. In [15], a phase-only synthesis technique was proposed to allow the MF design of a reflectarray by optimizing the antenna functioning over a certain bandwidth. The broadband beam-steering problem in conformal arrays was also addressed in [16], by applying the time reversal technique, which takes the Fourier transform of the time reversed version of the received signals. Unfortunately, its applicability is limited to the pattern beam-steering and the DRR is not taken into account. In [17], a multiobjective evolutionary algorithm was developed to synthesize wideband conformal arrays by determining the positions and excitations of the elements to minimize the side-lobe level (SLL) at different scan directions and frequencies.

This overview reveals that several array processing algorithms are currently available, but the design of a technique jointly allowing MF beam/null synthesis, phase-only control, DRR reduction, and applicability to conformal structures still represents an open problem. Therefore, to address this issue, this article proposes a synthesis method enabling MF phase-only and DRR controls for antenna arrays in which the geometry, the number of elements, and the single-element patterns are all arbitrary. The method, which extends the preliminary solution developed in [18], relies on the alternating projection approach [19] to optimize the array excitation vectors at the desired frequencies in agreement with the assigned pattern masks. The optimized vectors share a common amplitude, controlled through a DRR constraint, and differ only for the phases, thus providing the required DRR and phase-only controls that simplify the realization of the feeding network. Furthermore, mutual coupling effects are included in the synthesis process with a wideband design that is achieved by selecting a proper number of sufficiently close discrete frequencies within the desired bandwidth. To prove the effectiveness of the introduced MF feature in capturing different characteristics of the monitored environment, the conceived algorithm is applied to some typical beamforming problems occurring in coastal monitoring scenarios. This task, which relies on accurate electromagnetic simulations, involves both small arrays of microstrip patch antennas and large arrays of circular open-ended waveguides, so as to check the suitability

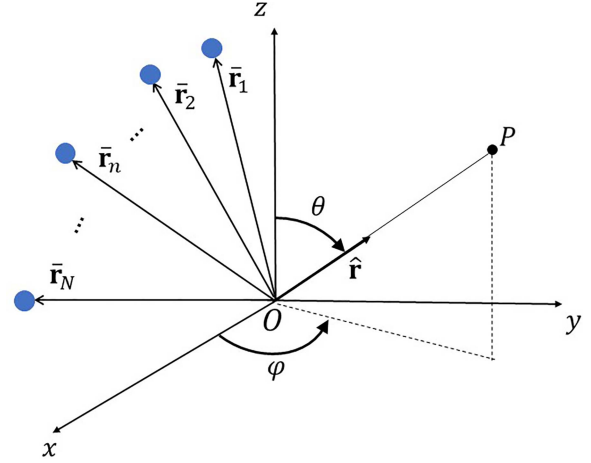


Fig. 1. Antenna array referred to a Cartesian system $O(x, y, z)$: P denotes the generic observation point having direction specified by the unit vector $\hat{\mathbf{r}}$, while $\bar{\mathbf{r}}_n$ for $n = 1, \dots, N$ represent the positions of the array elements (identified by blue dots).

of the proposed solution on operating vehicles of different sizes.

The rest of this article is organized as follows. Section II introduces the addressed problem. Section III describes the developed algorithm. Section IV discusses the numerical results. Finally, Section V concludes this article.

II. PROBLEM FORMULATION

Let us consider an antenna array of arbitrary geometry composed by N elements (see Fig. 1). With reference to a Cartesian system $O(x, y, z)$, let $\bar{\mathbf{r}}_n = x_n \hat{\mathbf{i}} + y_n \hat{\mathbf{j}} + z_n \hat{\mathbf{k}}$ be the position of the n th element, $\hat{\mathbf{i}}, \hat{\mathbf{j}}, \hat{\mathbf{k}}$ being the unit vectors of the Cartesian axes. Besides, the generic direction of observation is denoted as $\hat{\mathbf{r}} = \sin \theta \cos \phi \hat{\mathbf{i}} + \sin \theta \sin \phi \hat{\mathbf{j}} + \cos \theta \hat{\mathbf{k}}$, and θ and ϕ are the zenith and azimuth angles, respectively. The radiation pattern of the antenna array at the direction $\hat{\mathbf{r}}$ and working frequency f can be expressed as

$$F(\mathbf{a}; f; \hat{\mathbf{r}}) = \sum_{n=1}^N a_n F_n(f; \hat{\mathbf{r}}) \quad (1)$$

where $\mathbf{a} = [a_1, \dots, a_N]$ is the (complex) vector of the excitations and $F_n(f; \hat{\mathbf{r}})$ is the embedded element pattern of the n th array element at the frequency f , i.e., the radiation pattern of the entire array with the excitation vector $\mathbf{e}_n = [0, \dots, 1, \dots, 0]$, having unity in the n th position and zero in others. The DRR of \mathbf{a} is defined as

$$\text{DRR}(\mathbf{a}) = \frac{\max_n |a_n|}{\min_n |a_n|} \quad (2)$$

which is in general larger than one. When (2) approaches unity, all the array elements have the same excitation amplitude and the efficiency of the antenna structure is maximized, but at the expense of its flexibility. In fact, the unity DRR strongly reduces the degrees of freedom of the problem and, in particular, the capability of realizing a fine control of the radiation pattern shape. This reduced flexibility can be partly overcome

by the use of the element positions as optimization variables, resulting in the so-called sparse or a-periodic isophoric array architectures [20], [21], [22]. However, the synthesis problem in these cases is by far more complicated, the control of the pattern shape is less accurate and the feeding design may be complicated by the irregular arrangement of the elements [23]. Indeed, in addition to the influence on the antenna efficiency, the DRR control in the case of periodic arrays may also lead to simpler feeding networks, whose practical realization can be a hard task and should hence be properly taken into account at the implementation stage.

The defined arbitrary array is required to work at S different frequencies f_1, \dots, f_S . More precisely, at the generic frequency f_s , the array pattern has to belong to a predefined mask $M_s = \{m_s(\hat{\mathbf{r}}) : M_s^{\text{low}}(\hat{\mathbf{r}}) \leq |m_s(\hat{\mathbf{r}})| \leq M_s^{\text{up}}(\hat{\mathbf{r}})\}$, where $M_s^{\text{low}}(\hat{\mathbf{r}})$ and $M_s^{\text{up}}(\hat{\mathbf{r}})$ are two positive functions representing its lower and upper bounds, respectively.

The problem considered in this article is that of finding S excitation vectors $\mathbf{a}_1, \dots, \mathbf{a}_S$, with $\mathbf{a}_s = [a_{1s}, \dots, a_{Ns}]$ for $s = 1, \dots, S$, which are able to produce radiation patterns belonging to the corresponding mask at each of the S desired frequencies. In addition to this requirement, the optimized vectors must be such that $|a_{n1}| = \dots = |a_{nS}|$ for $n = 1, \dots, N$, i.e., the excitation amplitude of each array element has to remain the same at all the S frequencies. Finally, the (common) excitation DRR must not exceed the prescribed value D_{max} . The overall mathematical problem can be formulated as follows.

Determine $\mathbf{a}_1, \dots, \mathbf{a}_S$ in such a way that

$$F(\mathbf{a}_s; f_s; \hat{\mathbf{r}}) \in M_s, \quad s = 1, \dots, S \quad (3a)$$

$$|a_{n1}| = |a_{n2}| = \dots = |a_{nS}| = \xi_n, \quad n = 1, \dots, N \quad (3b)$$

$$\text{DRR}(\boldsymbol{\xi}) \leq D_{\text{max}} \quad (3c)$$

where condition (3a) imposes that the pattern at each frequency belongs to the prescribed mask, condition (3b) imposes that the excitation amplitude is the same at the S frequencies but can be different among the elements, while, finally, condition (3c) imposes that the DRR of the excitations does not exceed the given threshold.

III. SYNTHESIS ALGORITHM

The developed algorithm is based on the alternating projection approach [24], which is an iterative procedure for determining a point belonging to the intersection between two sets. To this aim, (3) must be first reformulated as an intersection finding problem. This operation requires the definition of the set \mathbf{W} , whose elements are given by

$$\tilde{\mathbf{w}} = \{\boldsymbol{\alpha}_1, \dots, \boldsymbol{\alpha}_S, \kappa_1(\hat{\mathbf{r}}), \dots, \kappa_S(\hat{\mathbf{r}})\} \quad (4)$$

where, for $s = 1, \dots, S$, $\boldsymbol{\alpha}_s = [\alpha_{1s}, \dots, \alpha_{Ns}]$ and $\kappa_s(\hat{\mathbf{r}})$ identify as arbitrary complex vectors and functions, respectively. Subsequently, inside \mathbf{W} , two subsets \mathbf{U} and \mathbf{V} are introduced, whose elements are given by

$$\begin{aligned} \tilde{\mathbf{u}} &= \{\mathbf{u}_1, \dots, \mathbf{u}_S, g_1(\hat{\mathbf{r}}), \dots, g_S(\hat{\mathbf{r}}) : g_s(\hat{\mathbf{r}}) \in M_s, \\ &= 1, \dots, S; \end{aligned}$$

$$|u_{n1}| = \dots = |u_{nS}| = \xi_n, \quad n = 1, \dots, N; \text{DRR}(\boldsymbol{\xi}) \leq D_{\text{max}} \quad (5)$$

$$\tilde{\mathbf{v}} = \{\mathbf{v}_1, \dots, \mathbf{v}_S, F(\mathbf{v}_1; f_1; \hat{\mathbf{r}}), \dots, F(\mathbf{v}_S; f_S; \hat{\mathbf{r}})\}. \quad (6)$$

In other words, the elements of \mathbf{W} are $2S$ -tuples composed by S arbitrary vectors having N complex elements and S arbitrary complex scalar functions. The elements of \mathbf{U} are instead composed by S complex vectors, which satisfy constraints (3b) and (3c), and by S scalar functions, which satisfy constraint (3a). Finally, the elements of \mathbf{V} are composed by S arbitrary complex vectors and the S patterns radiated by the adopted array at the S selected frequencies. These settings imply that the elements of \mathbf{V} satisfy the array equation in (1), but not the constraints in (3). An acceptable solution for the formulated problem has hence to belong to both sets \mathbf{U} and \mathbf{V} . This leads to the requested intersection finding problem, which can be solved through the alternating projection approach by preliminarily defining the squared distance between two elements $\tilde{\mathbf{w}}, \tilde{\mathbf{w}}' \in \mathbf{W}$ as

$$\rho^2(\tilde{\mathbf{w}}, \tilde{\mathbf{w}}') = \sum_{s=1}^S [\|\boldsymbol{\alpha}_s - \boldsymbol{\alpha}'_s\|_E^2 + \|\kappa_s(\hat{\mathbf{r}}) - \kappa'_s(\hat{\mathbf{r}})\|^2] \quad (7)$$

where $\|\cdot\|_E$ represents the Euclidean norm and $\|\cdot\|$ denotes the mean-square norm. Using (7), the projector of point $\tilde{\mathbf{w}}$ onto the set $\mathbf{X}(\subset \mathbf{W})$ can be defined as

$$\begin{aligned} \mathcal{P}_{\mathbf{X}} : \mathbf{W} &\rightarrow \mathbf{X} \\ \tilde{\mathbf{w}} &\mapsto \tilde{\mathbf{x}} = \arg \min_{\tilde{\mathbf{x}} \in \mathbf{X}} \rho(\tilde{\mathbf{w}}, \tilde{\mathbf{x}}). \end{aligned} \quad (8)$$

By consequence, this projector associates to $\tilde{\mathbf{w}}$ the point(s) $\tilde{\mathbf{x}}$ of \mathbf{X} having the minimum distance from $\tilde{\mathbf{w}}$. The specific expressions of the projector operators $\mathcal{P}_{\mathbf{U}}$ and $\mathcal{P}_{\mathbf{V}}$ are derived in the following subsections. In this regard, it may be worth to emphasize that, if the set \mathbf{X} is closed, such a projection point exists, and, if \mathbf{X} is also convex, the projection is unique. Otherwise, if \mathbf{X} is not convex, more than one point could exist and a proper selection procedure must be defined. With reference to the here addressed problem, it is evident from (5) and (6) that \mathbf{V} is convex, but \mathbf{U} is not because of the mask constraints [25].

Once the projection operators are characterized, the iterative procedure

$$\tilde{\mathbf{u}}_{n+1} = \mathcal{P}_{\mathbf{U}}[\mathcal{P}_{\mathbf{V}}(\tilde{\mathbf{u}}_n)], \quad n = 0, 1, 2, \dots \quad (9)$$

may be introduced to find a point belonging to the intersection $\mathbf{U} \cap \mathbf{V}$ by starting from a suitable point $\tilde{\mathbf{u}}_0 \in \mathbf{U}$. Thanks to the properties of the projector in (8) and of the distance in (7), the sequence of distances from $\tilde{\mathbf{u}}_n$ to \mathbf{V} is nonincreasing, thus it converges to a point of \mathbf{U} minimizing the distance from \mathbf{V} . As previously discussed, \mathbf{U} is nonconvex, and, in addition, the intersection $\mathbf{U} \cap \mathbf{V}$ might be empty. For this reason, a termination criterion must be introduced. This criterion states that iteration (9) is stopped when

$$\rho(\tilde{\mathbf{u}}_n, \mathbf{V}) < \varepsilon \quad \text{or} \quad \frac{\rho(\tilde{\mathbf{u}}_{n-1}, \mathbf{V}) - \rho(\tilde{\mathbf{u}}_n, \mathbf{V})}{\rho(\tilde{\mathbf{u}}_n, \mathbf{V})} < \delta \quad (10)$$

where ε and δ are two suitable thresholds. Beside the termination criterion, due to the nonconvexity of \mathbf{U} , also a choice criterion

must be adopted when more than one projection point is found. The most suitable choice criterion (which is not critical [8]) depends on the application and is not discussed here. When the iteration is stopped, the S vectors of $\tilde{\mathbf{u}}$ are chosen as the optimal excitation vectors. With this choice, the phase-only control is ensured, as well as the DRR reduction, which are required by constraints (3b) and (3c), respectively. On the other hand, it may be worth to remark that, due to the definition (5) of the set U , the S scalar functions of $\tilde{\mathbf{u}}$ satisfy constraint (3a), but have no relation with the antenna array. Thus, the patterns radiated by the array when excited by the optimal excitation vectors at the S considered frequencies might, in general, not strictly belong to the masks (unless $\rho(\tilde{\mathbf{u}}_n, \mathbf{V}) = 0$). However, as it will be shown in Section IV, really satisfactory patterns are typically obtained, denoting that constraint (3a) is closely approached.

A. Projector \mathcal{P}_U

Given the point $\tilde{\mathbf{w}} = \{\alpha_1, \dots, \alpha_S, \kappa_1(\hat{\mathbf{r}}), \dots, \kappa_S(\hat{\mathbf{r}})\} \in \mathbf{W}$, the projection of $\tilde{\mathbf{w}}$ onto the set U is the point $\tilde{\mathbf{u}} \in U$ that minimizes the squared distance $\rho^2(\tilde{\mathbf{w}}, \tilde{\mathbf{u}})$ in (7). Following the analysis in [24], the vectors \mathbf{u}_s , for $s = 1, \dots, S$, can be found as

$$\angle u_{ns} = \angle \alpha_{ns}, \quad n = 1, \dots, N; s = 1, \dots, S \quad (11)$$

$$|\xi'_n| = \frac{1}{S} \sum_{s=1}^S |\alpha_{ns}|, \quad n = 1, \dots, N. \quad (12)$$

Now, if $\text{DRR}(\xi') \leq D_{\max}$, then $|u_{ns}| = \xi'_n$ for $s = 1, \dots, S$. However, the vector $\xi' = [\xi'_1, \dots, \xi'_N]$ derived by (12) might not satisfy condition (3c). When this event occurs, the procedure described in [26] can be used to obtain a vector ξ such that $\text{DRR}(\xi) \leq D_{\max}$ and $|u_{ns}| = \xi_n$ for $s = 1, \dots, S$. Accordingly, the functions $g_s(\hat{\mathbf{r}})$ that minimize $\rho^2(\tilde{\mathbf{w}}, \tilde{\mathbf{u}})$ can be expressed as

$$g_s(\hat{\mathbf{r}}) = \begin{cases} M_s^{\text{low}}(\hat{\mathbf{r}}) \frac{g_s(\hat{\mathbf{r}})}{|g_s(\hat{\mathbf{r}})|}, & \text{if } |g_s(\hat{\mathbf{r}})| < M_s^{\text{low}}(\hat{\mathbf{r}}) \\ M_s^{\text{up}}(\hat{\mathbf{r}}) \frac{g_s(\hat{\mathbf{r}})}{|g_s(\hat{\mathbf{r}})|}, & \text{if } |g_s(\hat{\mathbf{r}})| > M_s^{\text{up}}(\hat{\mathbf{r}}) \\ g_s(\hat{\mathbf{r}}), & \text{otherwise} \end{cases} \quad (13)$$

which completes the evaluation of $\tilde{\mathbf{u}} = \mathcal{P}_U[\tilde{\mathbf{w}}]$.

B. Projector \mathcal{P}_V

Given the point $\tilde{\mathbf{w}} = \{\alpha_1, \dots, \alpha_S, \kappa_1(\hat{\mathbf{r}}), \dots, \kappa_S(\hat{\mathbf{r}})\} \in \mathbf{W}$, the projection of $\tilde{\mathbf{w}}$ onto the set V is the point $\tilde{\mathbf{v}} \in V$ that minimizes the squared distance $\rho^2(\tilde{\mathbf{w}}, \tilde{\mathbf{v}})$ in (7). Thanks to the definition of the set V in (6), $\rho^2(\tilde{\mathbf{w}}, \tilde{\mathbf{v}})$ can be expressed as a function of the vectors \mathbf{v}_s , which, after some manipulations, may be written as

$$\mathbf{v}_s = [\mathbf{I} + \mathbf{J}_s]^\dagger (\mathbf{h}_s + \alpha_s), \quad s = 1, \dots, S \quad (14)$$

where $[\cdot]^\dagger$ denotes the matrix pseudo inverse [27], \mathbf{I} is the $N \times N$ identity matrix, and $\mathbf{J}_s = [F_{mn}^s]$, with

$$F_{mn}^s = \int_{\Omega} F_n(f_s; \hat{\mathbf{r}}) F_m^*(f_s; \hat{\mathbf{r}}) d\Omega, \quad n, m = 1, \dots, N \quad (15)$$

$$h_{sn} = \int_{\Omega} \kappa_s(\hat{\mathbf{r}}) F_n^*(f_s; \hat{\mathbf{r}}) d\Omega, \quad n = 1, \dots, N \quad (16)$$

where $[\cdot]^*$ denotes the complex conjugate. Once the vectors \mathbf{v}_s are calculated by (14), the projection $\tilde{\mathbf{v}} = \mathcal{P}_V[\tilde{\mathbf{w}}]$ can be evaluated by using the definition of the set V in (6).

IV. NUMERICAL EXAMPLES

This section presents two numerical examples to check the effectiveness of the proposed method, which is implemented in Matlab R2022b on a personal laptop equipped with an Intel Core2 i7-12800H CPU at 2.40 GHz with 32 GB RAM. The examples involve MF phase-only pattern synthesis problems applied to a dual-frequency linear array working in C- and X-band and to a large X-band multiring antenna array. In both cases, the upper and lower bounds of the masks are identified by piecewise linear functions. Concerning the starting point (whose choice is indeed not critical [8]), the S vectors of $\tilde{\mathbf{u}}_0$ are zero vectors, while the corresponding S functions are the lower bounds of the masks. The thresholds $\varepsilon = \delta = 10^{-6}$ are selected for the termination condition in (10), and the `pinv` Matlab function is used with its default setting for the evaluation of the pseudo-inverse in (14).

A. Example 1: Uniform Linear Array of Patch Antennas

The first example considers, as single array element, a comb-slot-loaded microstrip patch antenna of edge $L = 14.5$ mm [Fig. 2(a)], whose structure relies on the design proposed in [6]. Precisely, the use of a comb-shaped slot, loaded on to a metallic patch allows one to obtain both electric and magnetic radiation characteristics, whose simultaneous usage improves the radiating performance. In addition, to achieve the desired electric and magnetic radiation, a modified L-probe feeding system with a capacitive matching ring arrangement is designed following the procedure described in [6].

The corresponding reflection coefficient, which is shown in Fig. 2(b), enables the radiator to operate at the $S = 2$ frequencies $f_1 = 6.5$ GHz and $f_2 = 11.1$ GHz, corresponding to the wavelengths $\lambda_1 = 46.5$ mm and $\lambda_2 = 26.9$ mm, respectively. The central frequency $f = 9$ GHz is instead not included, since the relative pattern is in this case inconsistent, as it often happens for some bands with multiband elements [6]. The complete structure, identifying a uniform linear array, consists of $N = 16$ radiators equally spaced on the x -axis and lying in the $x - y$ plane [Fig. 2(c)]. The interelement distance, i.e., the distance between the centers of two adjacent patches, is equal to $d = 15.3$ mm (corresponding to $0.33\lambda_1$ and $0.57\lambda_2$). With these choices, the overall antenna array has a planar, compact, lightweight structure with potential application in many airborne and autonomous aircraft vehicle (UAV) technologies. In addition, the dual frequency capability, allows the antenna to be suitable for different applications. In fact, the lower frequency f_1 belongs to the C-band and is suitable for aeronautical radio navigation, in particular for airborne radar altimeter as well as for airborne vehicle telecommand, telemetry, and radio proximity fuse applications. Moreover, the higher frequency f_2 belongs to the X-band and is typically used for synthetic aperture radar

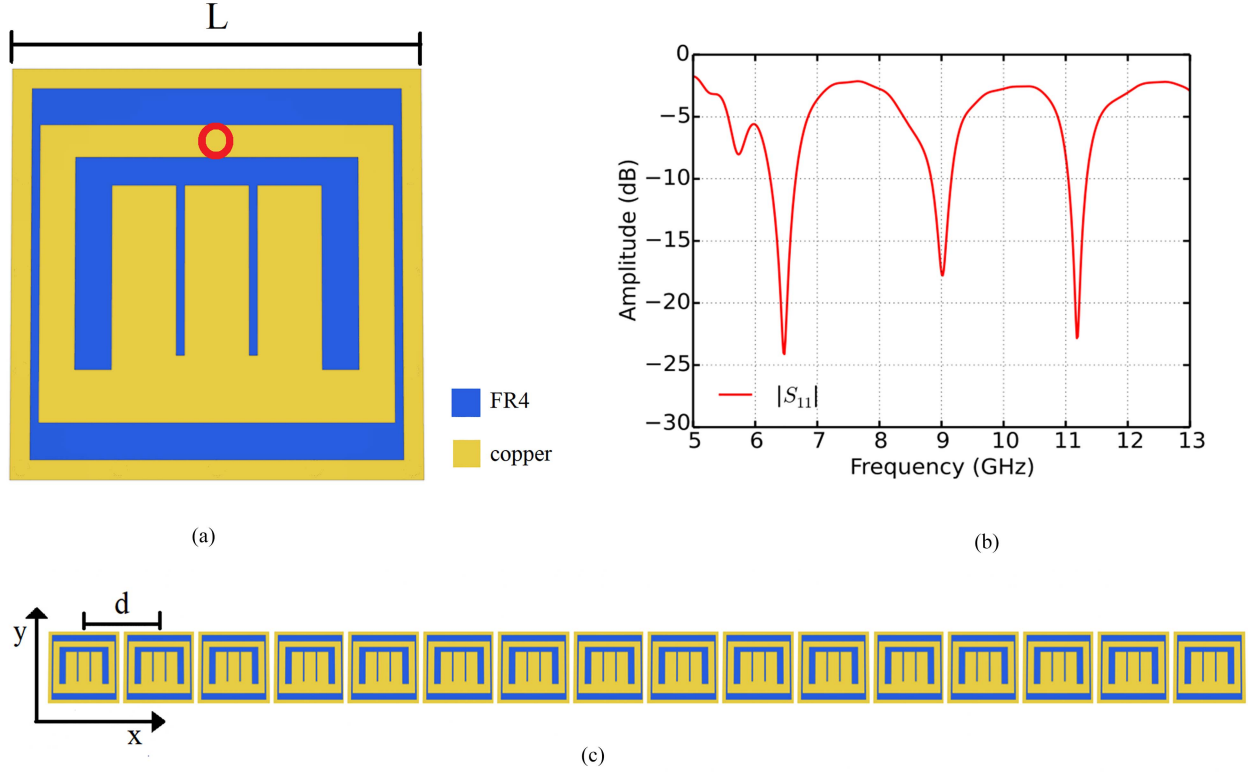


Fig. 2. Example 1 - Comb-slot-loaded microstrip patch antenna array. (a) Single element (blue and yellow colors identify FR4 and copper, respectively, red dot represents the position of the capacitive matching ring used in the L-probe feeding system from the metallic bottom layer). (b) Reflection coefficient. (c) Antenna array.

TABLE I
EXAMPLE 1 - OPTIMIZED EXCITATION VECTORS (IN AMPLITUDE AND PHASE) IN THE ABSENCE OF DRR CONSTRAINTS

n	1	2	3	4	5	6	7	8	9	10	11	12	13	14	15	16
ξ_n	1.22	0.95	1.10	1.00	1.12	1.63	1.48	1.59	1.49	1.36	1.48	1.14	1.14	1.13	0.63	1.08
$\angle u_{n1}$	-91.2°	-7.7°	-92.3°	-66.1°	-41.9°	-99.7°	-21.6°	-84.1°	-80.4°	-34.9°	-99.9°	-32.3°	-61.7°	-91.9°	-22.0°	-80.1°
$\angle u_{n2}$	-94.9°	-108.3°	-82.7°	-97.4°	-96.5°	-96.6°	-96.2°	-95.4°	-95.0°	-95.4°	-96.3°	-97.4°	-98.8°	-81.1°	-112.1°	-95.5°

(SAR) imaging and for low-cost compact microwave remote sensing. Further antenna elements operating in these frequency bands may be found in [28], [29], [30], and [31]. The embedded element patterns $F_n(f_s; \theta)$, with θ denoting the angle from the array axis, are evaluated for $n = 1, \dots, 16$ and $s = 1, 2$ in the positive $x - z$ half plane by using the electromagnetic simulator CST Microwave Studio Suite [32], to properly account for the mutual coupling effects among the radiators. The maximum gains at f_1 and f_2 are 4.32 and 1.64 dBi, respectively. The $S = 2$ masks are subsequently defined to have a pencil-beam shape with a pointing direction at $\theta_d = 90^\circ$ and a -20 dB SLL. In addition to these requirements, the first mask is conceived to impose a null at $\theta_n = 125^\circ$ to reject possible interferers incoming from that direction or to suppress reflections from an ambiguous region.

The first set of results is derived by applying the developed algorithm in the absence of DRR constraints. The obtained normalized patterns as a function of the zenith angle are reported in

Fig. 3, while the optimized excitation vectors are listed in Table I. The values in the table further reveal that this performance is achieved by adopting a common DRR, approximately equal to 2.57. The curves in the figure show that the shape of the synthesized patterns properly match all the three requirements imposed by the defined masks: 1) main-lobe shape, 2) SLL, and 3) null depth. In strict mathematical terms, constraint (3b) is of course rigorously satisfied, while constraint (3a) is really closely approached.

The maximum gains obtained by these configurations are 13.1 dBi at f_1 and 16.0 dBi at f_2 . Regarding this first solution, it is worth to observe that the higher the DRR value, the higher the amplitude unbalance and the mutual coupling effects among the antenna elements. The first aspect might strongly complicate the realization of the feeding network, requiring a careful power division system design or, in the case of active arrays, the need for different levels of operation for the power amplifiers, which cannot operate at the same (optimal) value. This mismatch

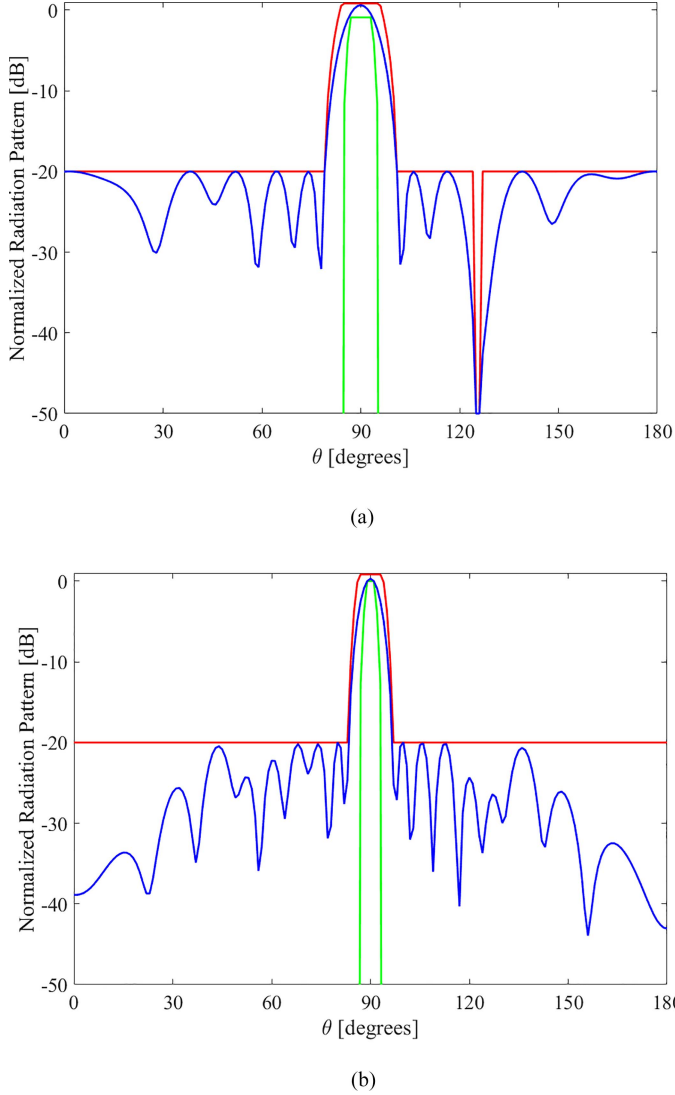


Fig. 3. Example 1 - Normalized patterns obtained at (a) $f_1 = 6.45$ GHz and (b) $f_2 = 11.14$ GHz in the absence of the DRR constraints (red line: mask upper bound, green line: mask lower bound, blue line: synthesized pattern). The piecewise-defined lower and upper bounds of the masks are characterized by the following values. $M_1^{\text{low}}(0^\circ) = M_1^{\text{low}}(84^\circ) = 10^{-8}$, $M_1^{\text{low}}(87^\circ) = M_1^{\text{low}}(93^\circ) = .9$, $M_1^{\text{low}}(96^\circ) = M_1^{\text{low}}(180^\circ) = 10^{-8}$; $M_1^{\text{up}}(0^\circ) = M_1^{\text{up}}(79^\circ) = 10^{-1}$, $M_1^{\text{up}}(85^\circ) = M_1^{\text{up}}(95^\circ) = 1.1$, $M_1^{\text{up}}(101^\circ) = M_1^{\text{up}}(180^\circ) = 10^{-1}$, $M_1^{\text{up}}(125^\circ) = 10^{-2.5}$; $M_2^{\text{low}}(0^\circ) = M_2^{\text{low}}(86^\circ) = 10^{-8}$, $M_2^{\text{low}}(89^\circ) = M_2^{\text{low}}(91^\circ) = 0.9$, $M_2^{\text{low}}(94^\circ) = M_2^{\text{low}}(180^\circ) = 10^{-8}$; $M_2^{\text{up}}(0^\circ) = M_2^{\text{up}}(83^\circ) = 10^{-1}$, $M_2^{\text{up}}(87^\circ) = M_2^{\text{up}}(93^\circ) = 1.1$, $M_2^{\text{up}}(97^\circ) = M_2^{\text{up}}(180^\circ) = 10^{-1}$.

might result in a significant loss of dc-to-RF efficiency, which is undesirable in power-sensitive scenarios, such as, for example, satellite communications and airborne radar [22]. Therefore, to partly reduce the DRR value and hence simplify the feeding network without excessively decreasing the number of available degrees of freedom of the array, the proposed algorithm is run again but in the presence of a DRR constraint with $D_{\text{max}} = 2$. This leads to the second set of results, corresponding to the normalized patterns reported in Fig. 4 and the excitation vectors listed in Table II. These curves and values reveal the capability of the presented method to maintain quite satisfactory pattern

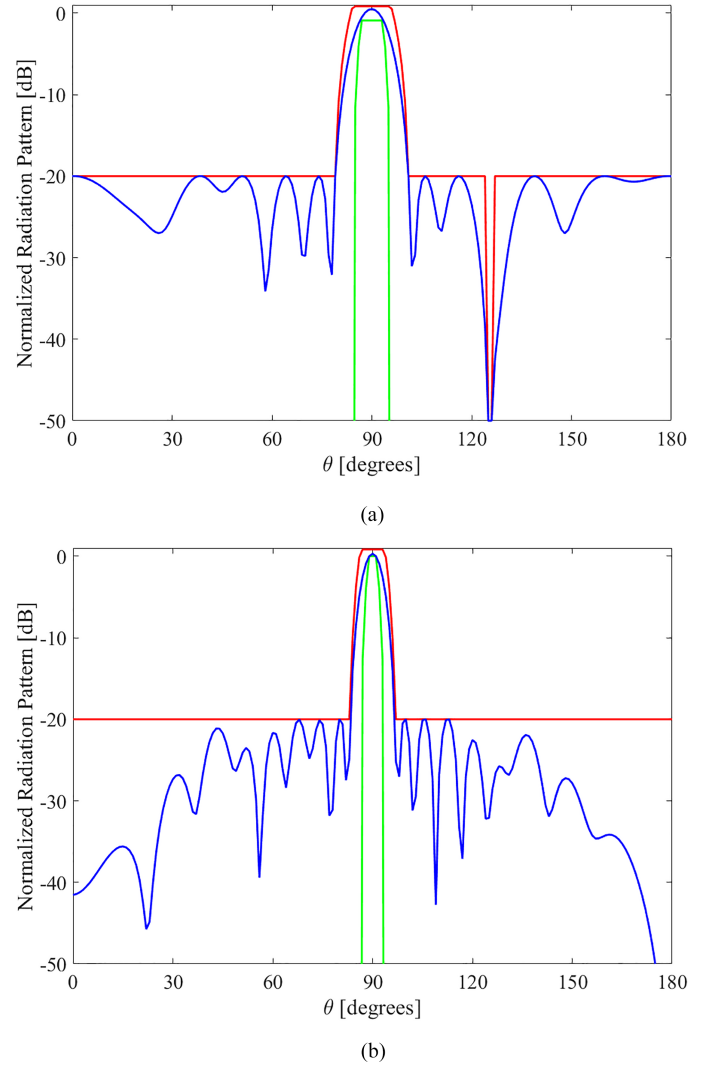


Fig. 4. Example 1 - Normalized patterns obtained at (a) $f_1 = 6.45$ GHz and (b) $f_2 = 11.14$ GHz for $D_{\text{max}} = 2$ (red line: mask upper bound, green line: mask lower bound, blue line: synthesized pattern).

shapes simultaneously reducing the DRR of the excitations. Furthermore, concerning the maximum gains, no degradation occurs, since 13.1 and 16.0 dBi are still obtained at f_1 and f_2 , respectively. Note that, according to the imposed phase-only control constraint, for both sets of results referred to this first example, the switch from one pattern to another requires the selection of the sole set of excitation phases, since the set of amplitudes, being unique, is common to the two patterns.

B. Example 2: Large Multiring Array of Isotropic Elements

The second example considers a concentric array lying on the $x - y$ plane and consisting of $N = 652$ evenly spaced radiators. More precisely, the elements are organized over $N_{\text{R}} = 16$ rings centered at the origin in such a way that the interelement distance is $d = \lambda_{\text{max}}/2$, where λ_{max} represents, among the S wavelengths involved in the synthesis process, the maximum one. The adopted geometry is shown in Fig. 5, while the ring radii and the number radiators over each ring are reported in Table III.

TABLE II
EXAMPLE 1 - OPTIMIZED EXCITATION VECTORS (IN AMPLITUDE AND PHASE) FOR $D_{\max} = 2$

n	1	2	3	4	5	6	7	8	9	10	11	12	13	14	15	16
ξ_n	1.21	0.95	1.05	0.98	1.17	1.57	1.50	1.55	1.53	1.35	1.52	1.13	1.17	1.12	0.78	1.01
$\angle u_{n1}$	-27.1°	58.5°	-27.4°	-4.8°	24.1°	-36.1°	42.8°	-21.6°	-16.2°	33.3°	-36.1°	35.5°	2.8°	-31.8°	42.4°	-18.4°
$\angle u_{n2}$	-0.1°	-15.0°	16.0°	-2.8°	-1.7°	-1.0°	-0.2°	0.1°	0.0°	-0.0°	-0.3°	-1.8°	-4.6°	17.4°	-19.2°	0.4°

TABLE III
EXAMPLE 2 - RADIUS AND NUMBER OF ELEMENTS OF EACH RING

Ring radius [cm]	2	4	6	8	10	12	14	16	18	20	22	24	26	28
Number of elements	6	12	18	25	31	37	43	50	56	62	69	75	81	87

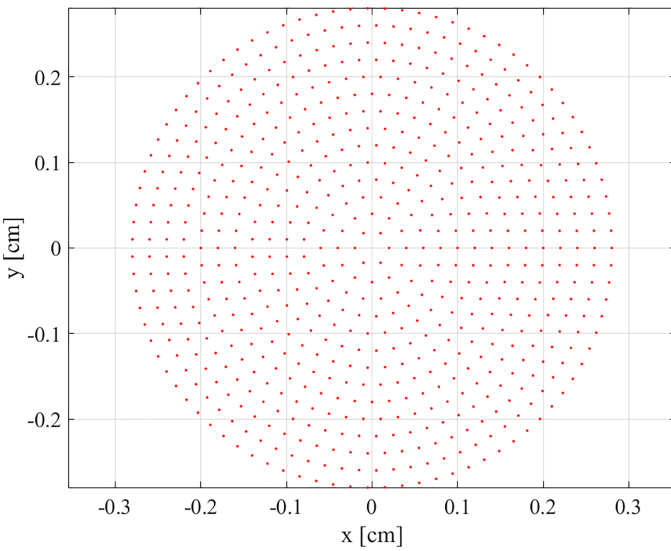


Fig. 5. Example 2 - Array geometry.

This physical system is required to cover a 50% bandwidth by operating at $S = 3$ equispaced frequencies: $f_1 = 7.5$ GHz, $f_2 = 10.0$ GHz, and $f_3 = 12.5$ GHz, corresponding to the wavelengths $\lambda_1 = \lambda_{\max} = 4.0$ cm, $\lambda_2 = 3.0$ cm, and $\lambda_3 = 2.4$ cm, respectively. These frequencies are often used in SAR imaging applications for the development of a low-power high-sensitivity X-band systems capable of imaging small radar-cross-section targets using very low transmitted power [33]. For the embedded elements, identical circular open-ended waveguides are assumed, whose patterns in (1) may be modeled according to [34] as

$$\begin{aligned}
 F_n(f_s; \hat{\mathbf{r}}) &= (\cos \theta)^{q_s} \exp \left[j \frac{2\pi}{\lambda_s} (x_n \sin \theta \cos \phi + y_n \sin \theta \sin \phi) \right], \\
 s &= 1, \dots, S; \quad n = 1, \dots, N
 \end{aligned} \quad (17)$$

where $q_s = 2.07[(d/\lambda_s)^2 - 0.5]$. The $S = 3$ masks are defined still considering the upper $x - z$ half plane and adopting a

pencil-beam shape, but now selecting $\theta_d = 0^\circ$ as pointing direction, and imposing a -30 dB SLL for $s = 1, 2$ and a -40 dB one for $s = 3$.

Similarly to the previous example, the algorithm is first used without DRR limitations, while subsequently it is run again by imposing increasingly stringent DRR constraints. In particular, a second set of simulations is carried out by selecting $D_{\max} = 4$ and a third one by imposing $D_{\max} = 1$. The three sets of resulting normalized patterns are reported in Fig. 6 as a function of θ , whose negative and positive values refer to the half-planes corresponding to the azimuth angles equal 180° and 0° , respectively. This representation has been preferred to the previous one to avoid the split of each main beam in two parts. The first three patterns in Fig. 6(a)–(c) reveal that, also for this scenario, constraint (3a) is approximated quite satisfactorily. However, this performance is obtained for a DRR approximately equal to 12.3 (the excitations in this case are not listed due to their large number), which may result too high for implementation purposes. For this reason, the adoption of DRR constraints becomes necessary. The second set of patterns in Fig. 6(d)–(f) shows that the shape and SLL requirements can be still properly satisfied by imposing a DRR lower than one third of the previous one, with significant benefits in terms of feeding network simplification. An acceptable behavior may also be observed in Fig. 6(g)–(i) for the limiting case corresponding to $D_{\max} = 1$, obtained applying the very stringent equiamplitude requirement. In fact, except for a moderate distortion of the main-lobe shape for f_2 and a slight overcoming of the required SLL for f_3 , all patterns are in very good agreement with the desired specifications. Therefore, in this second application, the pattern switching is not only enabled by phase-only control, as in the previous example, but, if the $D_{\max} = 1$ solution is chosen, might be even realized just using phase shifters and completely avoiding the precise design of unbalanced power dividers, since the amplitudes would be all unitary. This solution, in addition to representing the simplest design, is also the most energy efficient one in the transmitting mode, since it allows all the amplifiers to work at their optimum. Finally, also in this second example the directivity values, which are listed in Table IV, are quite satisfactory and do not experience significant modifications as the DRR constraint becomes more stringent.

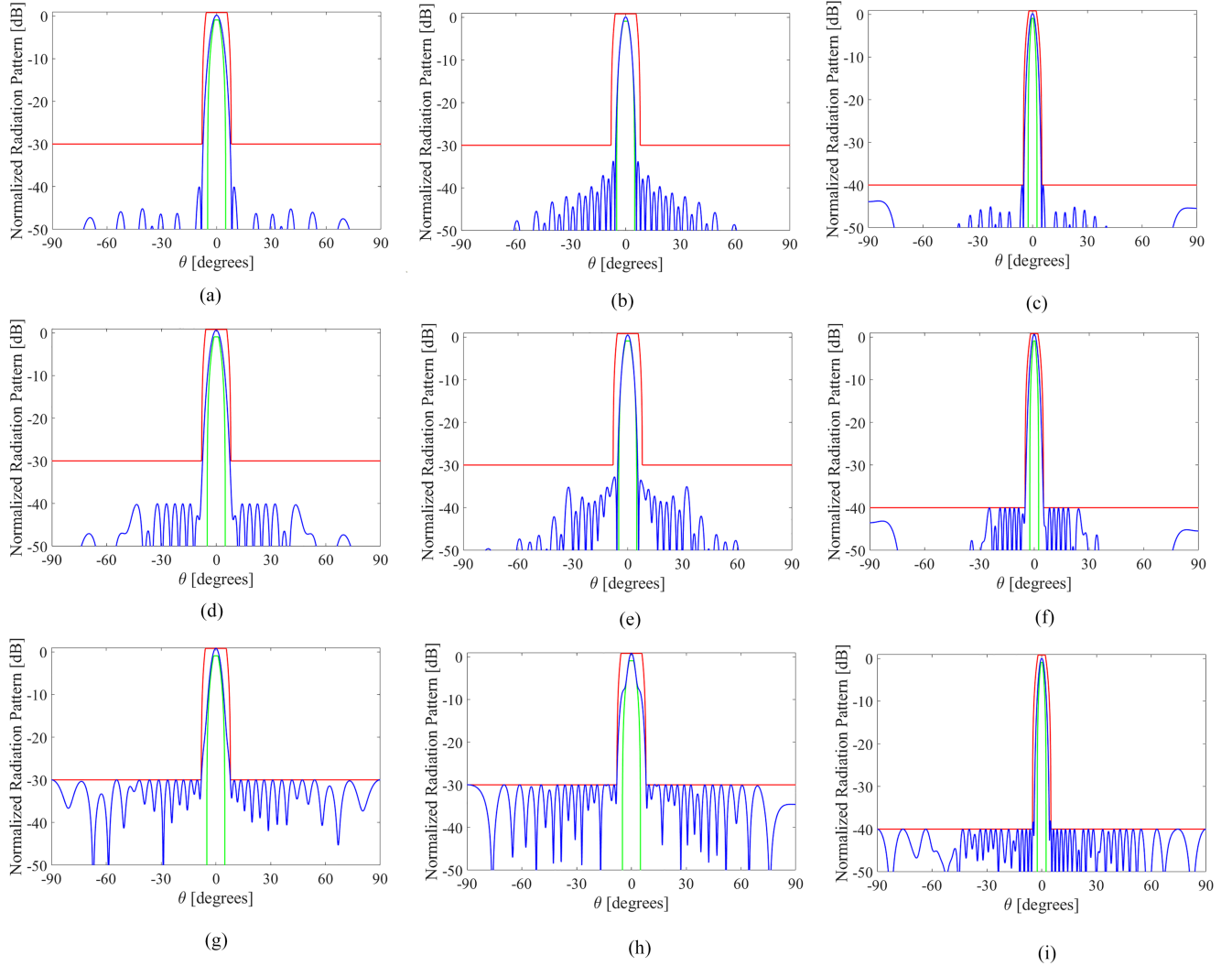


Fig. 6. Example 2 - Normalized patterns obtained at (a), (d), (g) $f_1 = 7.5$ GHz, (b), (e), (h) $f_2 = 10.0$ GHz, and (c), (f), (i) $f_3 = 12.5$ GHz in the absence of (a)–(c) DRR constraints, for (d)–(f) $D_{\max} = 4$, and for (g)–(i) $D_{\max} = 1$ (red line: mask upper bound, green line: mask lower bound, blue line: synthesized pattern). The piecewise-defined lower and upper bounds of the masks are characterized by the following values. $M_s^{\text{low}}(-90^\circ) = M_s^{\text{low}}(-5^\circ) = 10^{-8}$, $M_s^{\text{low}}(-1.25^\circ) = .9$; $M_s^{\text{up}}(-90^\circ) = M_s^{\text{up}}(-8^\circ) = 10^{-1.5}$, $M_s^{\text{up}}(-5.75^\circ) = 1.1$; $s = 1, 2$; $M_3^{\text{low}}(-90^\circ) = M_3^{\text{low}}(-2.5^\circ) = 10^{-8}$, $M_3^{\text{low}}(-0.5^\circ) = .9$; $M_3^{\text{up}}(-90^\circ) = M_3^{\text{up}}(-5^\circ) = 10^{-2}$, $M_3^{\text{up}}(-2^\circ) = 1.1$.

TABLE IV
EXAMPLE 2 - DIRECTIVITY VALUES IN dBi

No DRR constraint			$D_{\max} = 4$			$D_{\max} = 1$		
$s = 1$	$s = 2$	$s = 3$	$s = 1$	$s = 2$	$s = 3$	$s = 1$	$s = 2$	$s = 3$
21.01	22.13	23.13	21.16	22.24	23.37	21.67	21.93	23.73

V. CONCLUSION

An innovative method of phase-only synthesis for MF conformal antenna arrays with DRR constraints has been proposed. The method allows the optimization of the element excitations in such a way that the power pattern of the array belongs to assigned masks at a given number of desired frequencies. Thanks to the phase-only constraint, the pattern switching at the different frequencies can be enabled by the dynamic selection of the sole

phases while maintaining the amplitudes unmodified, whose DRR may be, in addition, controlled during the optimization process. This provides a certain versatility to the conceived method, thus enabling a positive tradeoff between pattern accuracy and implementation simplicity. Beside these aspects, the numerical results have further revealed the capability of the developed solution to account for the mutual coupling effects between the radiators and to operate on large arrays with hundreds of elements by adopting even unitary excitation amplitudes.

REFERENCES

- [1] D. Chen and J. A. Nanzer, "Analysis of imageless ground scene classification using a millimeter-wave dynamic antenna array," *IEEE Trans. Geosci. Remote Sens.*, vol. 60, 2022, Art. no. 2004710.
- [2] J. F. Vesecky, K. Laws, and J. D. Paduan, "Monitoring of coastal vessels using surface wave HF radars: Multiple frequency, multiple site and multiple antenna considerations," in *Proc. IEEE Int. Geosci. Remote Sens. Symp.*, Jul. 2008, vol. 1, pp. 1-405–1-408.

- [3] O. A. Iupikov, M. V. Ivashina, C. Cappellin, and N. Skou, "Digital-beamforming array antenna technologies for future ocean-observing satellite missions," in *Proc. IEEE Int. Symp. Antennas Propag.*, Jun./Jul. 2016, pp. 1377–1378.
- [4] C. D. Curtis, M. Yeary, and J. L. Lake, "Adaptive nullforming to mitigate ground clutter on the national weather radar testbed phased array radar," *IEEE Trans. Geosci. Remote Sens.*, vol. 54, no. 3, pp. 1282–1291, Mar. 2016.
- [5] C. Fulton et al., "Cylindrical polarimetric phased array radar: Beamforming and calibration for weather applications," *IEEE Trans. Geosci. Remote Sens.*, vol. 55, no. 5, pp. 2827–2841, May 2017.
- [6] S. E. Valavan, D. Tran, A. G. Yarvoy, and A. G. Roederer, "Planar dual-band wide-scan phased array in X-band," *IEEE Trans. Antennas Propag.*, vol. 62, no. 10, pp. 5370–5375, Oct. 2014.
- [7] C. Cappellin et al., "Novel multi-beam radiometers for accurate ocean surveillance," in *Proc. Eur. Conf. Antennas Propag.*, Apr. 2014, pp. 3531–3535.
- [8] G. Buttazzoni and R. Vescovo, "Power synthesis for reconfigurable arrays by phase-only control with simultaneous dynamic range ratio and near-field reduction," *IEEE Trans. Antennas Propag.*, vol. 60, no. 2, pp. 1161–1165, Feb. 2012.
- [9] A. Tanner, T. Gaier, W. Imbriale, P. Kangaslahti, B. Lambrigtsen, and B. Lim, "A dual-gain design for the geostationary synthetic thinned array radiometer," *IEEE Geosci. Remote Sens. Lett.*, vol. 11, no. 8, pp. 1340–1344, Aug. 2014.
- [10] W. Bu-hong and G. Ying, "Frequency-invariant pattern synthesis for conformal array with space-time-polarization weighting structure," in *Proc. IEEE Int. Symp. Antennas Propag.*, Jul. 2008, pp. 1–4.
- [11] Y. Liu, Y. Yang, F. Han, Q. H. Liu, and Y. J. Guo, "Improved beam-scannable ultra-wideband sparse antenna arrays by iterative convex optimization based on raised power series representation," *IEEE Trans. Antennas Propag.*, vol. 68, no. 7, pp. 5696–5701, Jul. 2020.
- [12] Y. Gong, S. Xiao, and B. Wang, "Synthesis of nonuniformly spaced arrays with frequency-invariant shaped patterns by sequential convex optimization," *IEEE Antennas Wireless Propag. Lett.*, vol. 19, no. 7, pp. 1093–1097, Jul. 2020.
- [13] L. Poli, N. Anselmi, M. Carlin, and P. Rocca, "Compressive sensing technique for multi-frequency sparse linear array design," in *Proc. Eur. Conf. Antennas Propag.*, Apr. 2015, pp. 1–3.
- [14] V. S. Gangwar, J. Kumari Modi, K. Sreenivasulu, A. K. Singh, and S. P. Singh, "Numerical analysis of multi-functional antenna array composed of differently sized elements," in *Proc. IEEE MTT-S Int. Microw. RF Conf.*, Nov. 2018, pp. 1–4.
- [15] A. Capozzoli, C. Curcio, A. Liseno, M. Migliorelli, and G. Toso, "Phase-only synthesis of conformal aperiodic reflectarrays with multi-frequency specifications," in *Proc. Eur. Conf. Antennas Propag.*, 2012, pp. 2220–2224.
- [16] D. Zhao, Y. Jin, B.-Z. Wang, and R. Zang, "Time reversal based broadband synthesis method for arbitrarily structured beam-steering arrays," *IEEE Trans. Antennas Propag.*, vol. 60, no. 1, pp. 164–173, Jan. 2012.
- [17] D. Bianchi, A. Monorchio, S. Genovesi, A. Corucci, D. H. Werner, and P. L. Werner, "The pareto optimization of wide-band conformal antenna arrays," in *Proc. IEEE Int. Symp. Antennas Propag.*, Jul. 2011, pp. 2427–2429.
- [18] G. Buttazzoni, E. Marongiu, F. Babich, A. Fanti, F. Vatta, and M. Comisso, "A method of synthesis for multi-frequency smart antenna arrays for coastal monitoring," in *Proc. IEEE Int. Workshop Metrology Sea*, Oct. 2023, pp. 37–41.
- [19] L. G. Gubin, B. T. Polyak, and E. V. Raik, "The method of projections for finding the common point of convex sets," *USSR Comput. Math. Math. Phys.*, vol. 7, no. 6, pp. 1–24, Jan. 1967.
- [20] A. F. Morabito and P. G. Nicolaci, "Optimal synthesis of shaped beams through concentric ring isophoric sparse arrays," *IEEE Antennas Wireless Propag. Lett.*, vol. 16, pp. 979–982, 2017.
- [21] G. Buttazzoni and R. Vescovo, "Density tapering of linear arrays radiating pencil beams: A new extremely fast gaussian approach," *IEEE Trans. Antennas Propag.*, vol. 65, no. 12, pp. 7372–7377, Nov. 2017.
- [22] L. Chen, Y. Liu, Y.-L. Ban, S. Yang, and Y. J. Guo, "Synthesis of large-scale planar isophoric sparse arrays using iterative least squares with nonredundant constraints (ILS-NRC)," *IEEE Trans. Antennas Propag.*, vol. 72, no. 5, pp. 4232–4245, May 2024.
- [23] D. Pinchera, M. D. Migliore, and G. Panariello, "Isophoric inflating deflating exploration algorithm (I-IDEA) for equal-amplitude aperiodic arrays," *IEEE Trans. Antennas Propag.*, vol. 70, no. 11, pp. 10405–10416, Nov. 2022.
- [24] R. Vescovo, "Reconfigurability and beam scanning with phase-only control for antenna arrays," *IEEE Trans. Antennas Propag.*, vol. 56, no. 6, pp. 1555–1565, Jun. 2008.
- [25] O. Bucci, G. D'Elia, G. Mazzarella, and G. Panariello, "Antenna pattern synthesis: A new general approach," *Proc. IEEE*, vol. 82, no. 3, pp. 358–371, Mar. 1994.
- [26] R. Vescovo, "Consistency of constraints on nulls and on dynamic range ratio in pattern synthesis for antenna arrays," *IEEE Trans. Antennas Propag.*, vol. 55, no. 10, pp. 2662–2670, Oct. 2007.
- [27] R. Horn and C. Johnson, *Matrix Analysis*. Cambridge, U.K.: Cambridge Univ. Press, 1992.
- [28] C. Livingstone, A. Gray, R. Hawkins, and R. Olsen, "CCRS C/X-airborne synthetic aperture radar: An R and D tool for the ERS-1 time frame," *IEEE Aerosp. Electron. Syst. Mag.*, vol. 3, no. 10, pp. 11–20, Oct. 1988.
- [29] P. H. Rao, S. Sujitha, and K. T. Selvan, "A multiband, multipolarization shared-aperture antenna: Design and evaluation," *IEEE Antennas Propag. Mag.*, vol. 59, no. 4, pp. 26–37, Aug. 2017.
- [30] M. Chen, X.-C. Fang, W. Wang, H.-T. Zhang, and G.-L. Huang, "Dual-band dual-polarized waveguide slot antenna for SAR applications," *IEEE Antennas Wireless Propag. Lett.*, vol. 19, no. 10, pp. 1719–1723, Oct. 2020.
- [31] A. Moreira, P. Prats-Iraola, M. Younis, G. Krieger, I. Hajnsek, and K. P. Papathanassiou, "A tutorial on synthetic aperture radar," *IEEE Geosci. Remote Sens. Mag.*, vol. 1, no. 1, pp. 6–43, Mar. 2023.
- [32] "CST computer simulation technology, studio suite," 2023.
- [33] G. L. Charvat, L. C. Kempell, and C. Coleman, "A low-power high-sensitivity X-band rail SAR imaging system [Measurement's Corner]," *IEEE Antennas Propag. Mag.*, vol. 50, no. 3, pp. 108–115, Jun. 2008.
- [34] Y. Rahmat-Samii, P. Cramer, K. Woo, and S. Lee, "Realizable feed-element patterns for multibeam reflector antenna analysis," *IEEE Trans. Antennas Propag.*, vol. 29, no. 6, pp. 961–963, Nov. 1981.



Giulia Buttazzoni (Senior Member, IEEE) received the M.Sc. degree (summa cum laude) in telecommunication engineering and the Ph.D. degree in information engineering from the University of Trieste, Trieste, Italy, in 2008 and 2013, respectively.

In 2014, she joined the Department of Engineering and Architecture, University of Trieste, where she is currently an Associate Professor of Electromagnetic Fields and Antennas. Her research interests include antenna array synthesis techniques and numerical methods for electromagnetic fields.

Dr. Buttazzoni is a Member of the Italian Electromagnetics Society and the National Inter-University Consortium for Telecommunications.



Fulvio Babich (Senior Member, IEEE) received the M.Sc. degree (summa cum laude) in electrical engineering from the University of Trieste, Trieste, Italy, in 1984.

He was with the Research and Development Laboratories, Telettra, Torrecuso, Italy, where he was engaged in optical fiber communications. Then, he joined Zeltron as a Communication System Engineer, responsible for the activities within the ESPRIT program. In 1992, he joined the Department of Engineering and Architecture, University of Trieste,

where he is currently a Full Professor of Digital Communications and Wireless Networks. He is also a Coordinator of the Ph.D. Board in Industrial and Information Engineering, University of Trieste. His research interests include wireless networks and millimeter-wave communications. He is involved in channel modeling, multiple access techniques, channel coding, error control techniques, and cross-layer design.

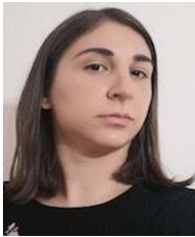
Dr. Babich is a member of the Board of National Telecommunications and Information Theory Group, and he was a member of the Directive Board of the National Inter-University Consortium for Telecommunications.



Alessandro Fanti (Senior Member, IEEE) received the M.Sc. degree in electronic engineering and the Ph.D. degree in electronic engineering and computer science from the University of Cagliari, Cagliari, Italy, in 2006 and 2012, respectively.

From 2013 to 2016, he was a Postdoctoral Fellow of the Electromagnetic Group, University of Cagliari, where he is currently an Assistant Professor. He has authored/coauthored 57 articles in international journals. His research interests include the use of numerical techniques for modes computation of guiding structures, optimization, analysis, and design of waveguide slot arrays and patch antennas, radio propagation in urban environments, modeling of bioelectromagnetic phenomena, and microwave exposure systems for biotechnology and bioagriculture.

Dr. Fanti is a member of the Italian Electromagnetics Society, the National Inter-University Consortium for Telecommunications, and the Interuniversity Center for the Interaction Between Electromagnetic Fields and Biosystems. He is an Associate Editor for IEEE JOURNAL OF ELECTROMAGNETICS, RF AND MICROWAVES IN MEDICINE AND BIOLOGY. He is a member of IEEE Antennas and Propagation Society. Since 2020, he has been a Principal Investigator of the IAPC Project, funded with C5 million by the Italian Ministry of Economic Development, within the AGRIFOOD PON I&C 2014–2020 (CUP: B21B1900064008 COR: 1406652).



Elena Marongiu (Student Member, IEEE) received the B.Sc. degree in electrical and electronic engineering and the M.Sc. degree in telecommunications engineering, in 2016 and 2019, respectively, from the University of Cagliari, Cagliari, Italy, where she is currently working toward the Ph.D. degree in electronic and computer engineering.

In 2020, she collaborated with the Italian Space Agency, Rome, Italy, on the Sardinia Deep Space Antenna optical configuration and radio telescope development in the X/K/Ka bands for near and deep space applications. Her research interests concern the modeling, analysis, and characterization of antennas, with specific reference to the design of microstrip antennas for radio-astronomical and 5G wearable devices.



Francesca Vatta (Member, IEEE) received the M.Sc. degree in electronic engineering and the Ph.D. degree in telecommunications from the University of Trieste, Trieste, Italy, in 1992 and 1998, respectively.

In 1999, she joined the Department of Engineering and Architecture, University of Trieste, where she is currently an Assistant Professor of Information Theory and Error-Control Coding. From 2002 to 2005, she has been a Visiting Scholar, respectively, with Notre Dame University, Notre Dame, IN, USA, cooperating with the Coding Theory Research Group (RG) under the guidance of Prof. D.J. Costello, Jr., and Ulm University, Ulm, Germany, cooperating with the telecommunications and applied information Theory RG under the guidance of Prof. M. Bossert. She has authored/coauthored more than 100 papers published in international journals and conference proceedings. Her research interests include channel coding concerning, in particular, the analysis and design of capacity-achieving codes.



Massimiliano Comisso (Member, IEEE) received the M.Sc. degree in electronic engineering and the Ph.D. degree in information engineering from the University of Trieste, Alcatel Trieste, Italy, in 2003 and 2007, respectively.

He was with Alcatel working on dense wavelength division multiplexin optical systems and with Danieli automation on electromagnetic non destructive examination modeling. He is currently an Associate Professor of Communication Networks and Waveguide/Optical Systems with the Department of Engineering and Architecture, University of Trieste. He has authored/coauthored more than 100 international scientific papers. His research interests include antenna array synthesis, small antennas, millimeter-wave communications, and distributed wireless networks.

Dr. Comisso was the Best Student Paper Award (BPA) Finalist at IEEE Global Communications Conference'06 and the recipient of the BPA at IEEE International Workshop on Computer Aided Modeling and Design of Communication Links and Networks'09. He serves as a referee/TPC Member for several IEEE journals and conferences.